Physica B 597 (2020) 412424

Contents lists available at ScienceDirect

Physica B: Physics of Condensed Matter

journal homepage: http://www.elsevier.com/locate/physb

Measuring current effect on low-temperature resistivity of *n*-type $Bi_{1.9}Lu_{0.1}Te_3$ compound: Probing the changing in conductivity mechanism under weak electric field

Oleg Ivanov [a,b,*], Maxim Yaprintsev [a], Roman Lyubushkin [b]

[a] Belgorod State University, Belgorod, 394015, Russia
[b] Belgorod State Technological University Named After V.G. Shukhov, Belgorod, 308012, Russia

ARTICLE INFO

Keywords:
Bismuth telluride
Electrical resistivity
Weak electric field
Conductivity mechanism
Electron mobilty
Hopping conductivity

ABSTRACT

The measuring current effect on low-temperature resistivity of $Bi_{1.9}Lu_{0.1}Te_3$ has been analyzed. Values of currents correspond to weak electric fields with strength of several $V \cdot m^{-1}$. Temperature behavior of the resistivity is connected to two mechanisms. High-temperature mechanism (above 35 K) is due to acoustic phonon scattering. For this mechanism, the resistivity is growing with both increasing temperature and increasing current (positive current effect). Low-temperature mechanism (below 35 K) results in appearance of resistivity minimum at low temperatures. Below the minimum, the resistivity is growing with decreasing temperature. This feature is originated from contribution from variable-range hopping conductivity. With increasing current, the resistivity is falling (negative current effect). Crossover from positive to negative current effect on the resistivity occurs with decreasing temperature. Positive effect is originated from saturation of drift velocity of electrons under electric field. Negative effect is due to activation of hopping conductivity via electric field.

1. Introduction

Ability of solids to conduct an electric current with density of j is known to be determined by their specific electrical conductivity, σ (or the specific electrical resistivity, $\rho = 1/\sigma$) [1]. In turn, for electron conductivity, σ is determined by electron concentration, n, and electron mobility, μ. Changing in n and/or μ, resulted from varying temperature of solid, its defect structure, presence of temperature gradient or various physical fields applied to solid and etc., will be characteristic and special features for different conductivity mechanisms. Usually, the measuring electric current (direct or alternating) is experimental parameter, governing the σ measuring. This current being constant during the σ measuring is related to a drift velocity of the electrons under external electric field, which is applied to a sample to measure σ. The electric current density and the electric field strength, E, can be transformed to each other via the Ohm law, $j = \sigma \cdot E$. Under weak electric field, when n, μ and, hence, σ are E-independent, an experimental $j(E)$ dependence obeys the Ohm law. In contrast, under strong electric field, n and/or μ start to be E-dependent, resulting in a deviation of the experimental $j(E)$ dependence from the Ohm law. However, although n and μ are really believed to be E-independent under weak electric field, minor changes in n and μ with varying E are seemed to take place and in this case [2–5]. This feature can be also used to characterize both conductivity mechanism and changing in the conductivity mechanism that is implemented in solid under specific experimental conditions.

The aim of this paper is to find and analyze the measuring current effect on features in low-temperature resistivity of *n*-type $Bi_{1.9}Lu_{0.1}Te_3$ compound, resulted from changing in conductivity mechanism, when the electric current density is corresponding to weak electric field. Bismuth telluride, Bi_2Te_3, as well as Bi_2Te_3-based alloys, are known to be most common thermoelectrics for low-temperature applications [6–8]. However, the thermoelectric efficiency of these thermoelectrics is not too high by now. To enhance the thermoelectric efficiency, doping with various elements is often and fruitfully applied [9–11]. Recently it was found that rare earth elements, R (R = Lu, Ce, Sm, Er, La, Gd, etc.), can be applied as effective dopants to remarkably enhance the thermoelectric performance of Bi_2Te_3 [12–20]. The $Bi_{1.9}Lu_{0.1}Te_3$ composition is known to be optimal one to maximize the thermoelectric efficiency of Lu-doped Bi_2Te_3 compounds [12,13]. Moreover, the Lu doping remarkably effects on the electrical properties of Bi_2Te_3, which become to be similar to that of inhomogeneous and disordered semiconductors [21–23]. Particularly, linear positive magnetoresistance and

* Corresponding author. Belgorod State University, Pobedy 85, Belgorod, 308015, Russia.
E-mail address: Ivanov.Oleg@bsu.edu.ru (O. Ivanov).

https://doi.org/10.1016/j.physb.2020.412424
Received 4 June 2020; Received in revised form 23 July 2020; Accepted 1 August 2020
Available online 7 August 2020

metal-semiconductor transition have been observed in $Bi_{1.9}Lu_{0.1}Te_3$ at low temperatures. So, $Bi_{1.9}Lu_{0.1}Te_3$ can be reasonably chosen as suitable object to study features in low-temperature electrical resistivity under weal electric field.

2. Materials and methods

Details of preparation and characterization of the samples being studied were earlier reported in Ref. [15]. In brief, to synthesize a starting $Bi_{1.9}Lu_{0.1}Te_3$ powder, the microwave-solvothermal synthesis was applied by using a MARS-6 microwave reactor at pressure of 4 MPa and temperature of 463 K for 15 min. To sinter bulk samples, the spark plasma sintering was applied by using a SPS-25/10 system at pressure of 40 MPa and temperature of 683 K for 5 min. According to XRD analysis, performed by a Rigaku Ultima IV diffractometer, the bulk samples were single phase with rhombohedral structure corresponding to the Bi_2Te_3 phase (Fig. 1). All the diffraction peaks in Fig. 1 can be indexed in accordance with space $R\bar{3}m$ symmetry (standard JCPDS 15–0863 card), and no remarkable impure phases such as tellurium, bismuth, lutetium or their other compounds are observed. To determine a correct elemental composition of the samples, a Shimadzu ICP emission ICPE-9000 spectrometer was applied. The Bi, Te and Lu concentrations were found to be equal to 38.07 at%, 59.95 at% and 1.98 at%, respectively. These concentrations are really corresponding to the $Bi_{1.9}Lu_{0.1}Te_3$ composition, and atomic (Bi + Lu)/Te ratio is equal to 2/3. A scanning electron microscope (SEM), Nova NanoSEM 450, was also applied to examine grain structure of the bulk samples. Disordered grain structure with grains having a crystal faceting and with average size of ~1160 nm was observed on SEM image of fractured surfaces of the samples (inset to Fig. 1). To estimate the average grain size, the histogram of the grain size distribution was plotted and analyzed in frames of the lognormal unimodal distribution.

To measure the specific electrical resistivity, rectangular bar samples with dimensions of 0.5 × 0.5 × 5 mm^3 were cut. Opposite faces of the bar, oriented perpendicularly to its long side, were covered by silver paste to measure a voltage drop across these faces. Mini Cryogen Free Measurements System (Cryogenic Ltd, UK) was applied to take ρ value

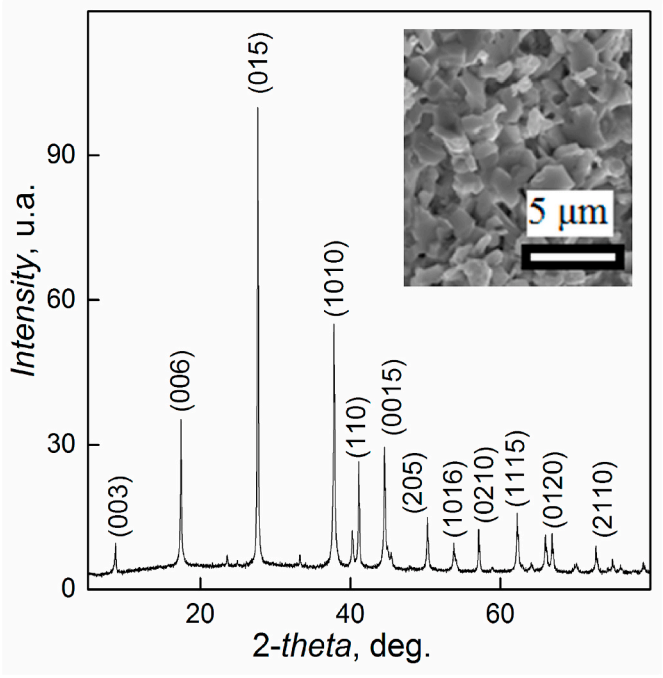

Fig. 1. The XRD pattern for the bulk $Bi_{1.9}Gd_{0.1}Te_3$ sample. Inset: the SEM image taken on the fractured surface of this sample.

by averaging voltage values, applied for forward and reverse current directions. Two measuring modes were involved. At the first measuring mode, the $\rho(T)$ dependences were taken at various values of current density. The j values were equal to $9{\cdot}10^4$, $29{\cdot}10^4$, $44{\cdot}10^4$, $88{\cdot}10^4$, $177{\cdot}10^4$ and $280{\cdot}10^4$ A m^{-2}. According to the second measuring mode, the $\rho(j)$ dependences were recordered at various temperatures equal to 2.5; 4; 6; 8; 10; 13; 16; 19; 23; 27; 30; 35; 40; 45; 50; 55 and 60 K, while j was gradually swept from $j_{min} = 9{\cdot}10^4$ A m^{-2} up to $j_{max} = 280{\cdot}10^4$ A m^{-2}. For detailed analysis of $\rho(j)$ features, the electric field strength corresponding to the measuring currents were calculated by the Ohm law. Owing to big length of the samples, E happened to be equal to a few of $V{\cdot}m^{-1}$ that is corresponding to weak electrical field. Thus, the electric current was used as direct experimental parameter effecting on ρ, whereas the electric field was calculated parameter, used to analyze the experimental data. The Hall effect was also examined to extract electron concentration and electron mobility.

3. Results and discussion

First of all, let us consider features in temperature behavior of the specific electrical resistivity, measured in accordance with the first measuring mode. The $\rho(T)$ dependences, taken for minimum ($9{\cdot}10^4$ A m^{-2}) and maximum ($280{\cdot}10^4$ A m^{-2}) values of the measuring current, are presented in Fig. 2 (a). To show a difference between these $\rho(T)$ curves more clearly, they are imaged by lines, but no experimental points. Obviously, that both dependences can be divided into high-temperature and low-temperature ranges. Characteristic temperature, separating these ranges, will be introduced later. Within the high-temperature range, ρ is steady decreasing with decreasing temperature that is characteristic of metals or degenerate semiconductors. Besides, although the $\rho(T)$ dependences taken for j_{min} and j_{max} are positioned very close to each other, i.e. the j-effect on ρ is rather weak, the $\rho(T)$ dependence for j_{max} is positioned a bit higher than the $\rho(T)$ dependence for j_{min} (inset to Fig. 2 (a)). In contrast to the $\rho(T)$ behavior, observed within the high-temperature range, ρ measured within the low-temperature range, firstly, behaves in more complicated manner, and, secondly, the j-effect on ρ is remarkably expressed. As temperature is gradually approaching to 2.5 K, the $\rho(T)$ dependence for j_{max} is steady tending to a saturated value, whereas for j_{min} a clear minimum is observed in the $\rho(T)$ dependence at $T_m \approx 11$ K. That is at T_m metal (ρ is decreasing with decreasing temperature) behavior in the electrical resistivity changes to semiconducting (ρ is increasing with decreasing temperature) behavior. It is important to note that within the low-temperature range, the $\rho(T)$ dependence for j_{min} is positioned remarkably higher than the $\rho(T)$ dependence for j_{max}, that is the j-effect on ρ for the low-temperature range is opposite to this effect for the high-temperature range.

To characterize this effect, one more quantity can be introduced as $DCR = [\rho(j_{max}) - \rho(j_{min})]/\rho(j_{min})$. Obviously, that DCR is similar to magnetoresistance, MR [24]. But, MR characterizes changes in the resistivity of solid being studied under varying magnetic field, whereas DCR characterizes changes in ρ with varying measuring current. The $DCR(T)$ dependence calculated is presented in Fig. 2 (b). This dependence summarizes all the features of the j-effect on ρ listed above. Thus, the j-effect on ρ has opposite sign and remarkably different magnitude for the low- (negative sign and strong effect) and high-temperature (positive sign and weak effect) ranges. Moreover, a magnitude of the negative j-effect on ρ is rapidly increasing with decreasing temperature. Crossover from the positive j-effect on ρ to the negative one takes place at $T_{cr} \approx 35$ K. The $\rho(T)$ curves taken for other j values are positioned between the $\rho(T)$ curves presented in Fig. 2 (a). For the high-temperature range, difference between the $\rho(T)$ curves taken at various j is very small to be reliably analyzed, whereas for the low-temperature range some patterns in behavior of the $\rho(T)$ minimum can be reliably extracted. Particularly, this minimum was found to be gradually depressed and shifted to lower temperatures, as j increases

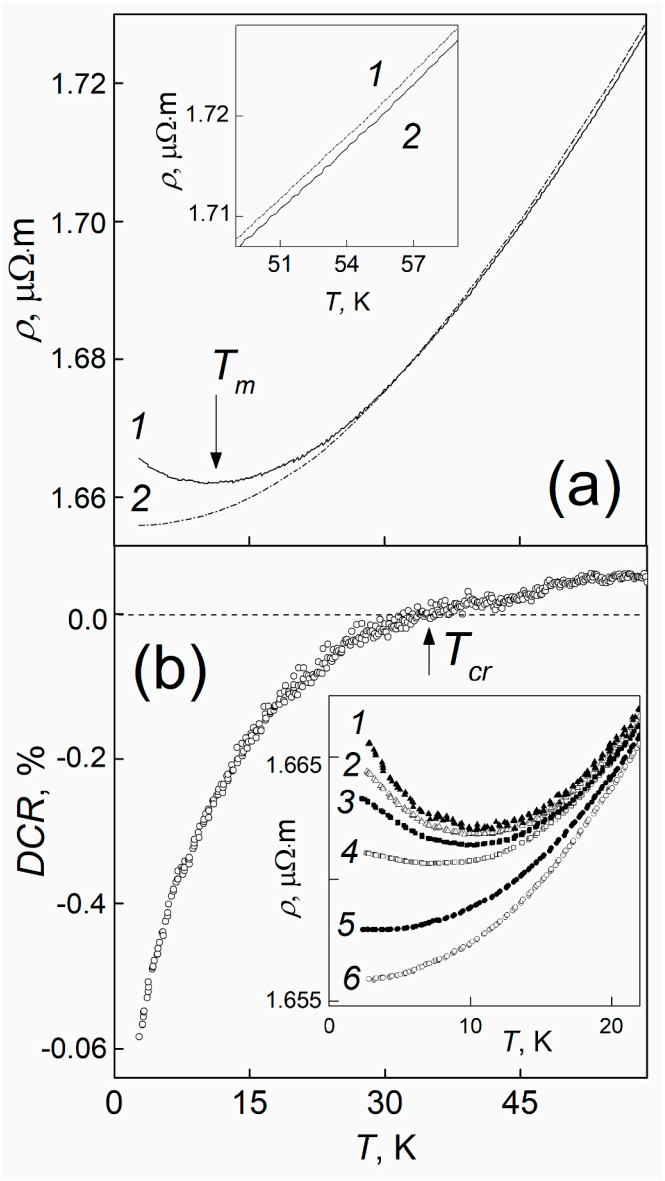

Fig. 2. (a) The $\rho(T)$ dependences taken at $j_{min} = 9{\cdot}10^4$ (curve *1*) and $j_{max} = 280{\cdot}10^4$ A·m^{-2} (*2*). Inset: large-scale high-temperature part of the same dependences, plotted to show a small difference in these dependences in detail. (b) The *DCR*(*T*) dependence, calculated by using the $\rho(T)$ dependences, shown in Fig. (a). Inset: the low-temperature $\rho(T)$ dependences taken at *j* equal to $9{\cdot}10^4$ (curve *1*) $29{\cdot}10^4$ (*2*), $44{\cdot}10^4$ (*3*), $88{\cdot}10^4$ (*4*) $177{\cdot}10^4$ (*5*) and $280{\cdot}10^4$ A m^{-2} (*6*).

from to $9{\cdot}10^4$ to $88{\cdot}10^4$ A m^{-2} (inset to Fig. 2 (b)). Just high-temperature part of the $\rho(T)$ minimum is observed for *j* equal $177{\cdot}10^4$ A m^{-2} and no ρ minimum can be found for j_{max}.

Appearing the low- and high-temperature ranges in the $\rho(T)$ dependences can be reasonably attributed to changing in conductivity mechanism from low-temperature mechanism, governing the low-temperature ρ behavior within the low-temperature range, to low-temperature mechanism, responsible for the high-temperature ρ behavior. Let us first consider the high-temperature mechanism. Since the majority current carriers in donor semiconductor are electrons, then its specific electrical resistance can be expressed as [1].

$$\rho = \frac{1}{en\mu} \tag{1}$$

where *e*, *n* and μ are the unit charge, the electron concentration and the electron mobility, respectively.

For metals and degenerate semiconductors, the electron concentration is known to be *T*-independent. To find the electron concentration for the compound being studied, the Hall effect was examined within the 2.5–60 K range. The Hall constant, R_H, happened to be *T*-independent and equal to ~ - $0.28{\cdot}10^{-6}$ cm^3·C^{-1}. The R_H constant has negative sign, since the majority current carriers are electrons. Then, taking into account link between R_H and *n*, $R_H = 1/(n{\cdot}e)$, the electron concentration was estimated as $n \approx 2.1{\cdot}10^{13}$ m^{-3}. The electron concentration is naturally *T*-independent similarly to R_H. As result, the $\rho(T)$ changes presented in Fig. 2 (a) should be dominantly resulted from temperature change in the electron mobility. For temperatures corresponding to the high-temperature range, the $\mu(T)$ behavior is related to scattering of electrons by acoustic phonons [1,25]. At acoustic vibrations, two neighboring atoms of the lattice vibrate in phase. These vibrations generate a deformation potential scattering. With increasing temperature, amplitude of the lattice vibrations is also increasing; thusly the carrier mobility is naturally decreasing. According to this scattering mechanism, the $\mu(T)$ dependence is expressed as

$$\mu = \frac{2\sqrt{2\pi}\, e\hbar^2 d v_s^2}{3m^{*5/2}(kT)^{3/2}D_{ac}^2} \tag{2}$$

where $\hbar$ is the Planck constant, *d* is the mass density, υ_s is the sound velocity, m* is the density-of-states effective mass, *k* is the Boltzmann constant and D_{ac} is the deformation potential.

The experimental $\rho(T)$ dependences taken at all the measuring currents were next replotted as the $\rho(T^{3/2})$ dependences. It was found that above some temperature, T_d, the replotted dependences are linear that is in accordance with expressions (1) and (2). For instance, the $\rho(T^{3/2})$ dependence for j_{max} is shown in Fig. 3. To correctly estimate T_d, the $d\rho/d(T^{3/2})$ derivative versus $T^{3/2}$ dependence was plotted (inset to Fig. 3). Value of this derivative is naturally constant above T_d, whereas just below T_d, the $d\rho/d(T^{3/2})$ vs. $T^{3/2}$ dependence starts to deviate from linear one. The T_d temperature, firstly, was estimated to be equal to ~35 K, and, secondly, this temperature was found to be *j*-independent. It should be noted that the T_d temperature is very well coinciding with the T_{cr} temperature, corresponding to the crossover from the positive *j*-effect

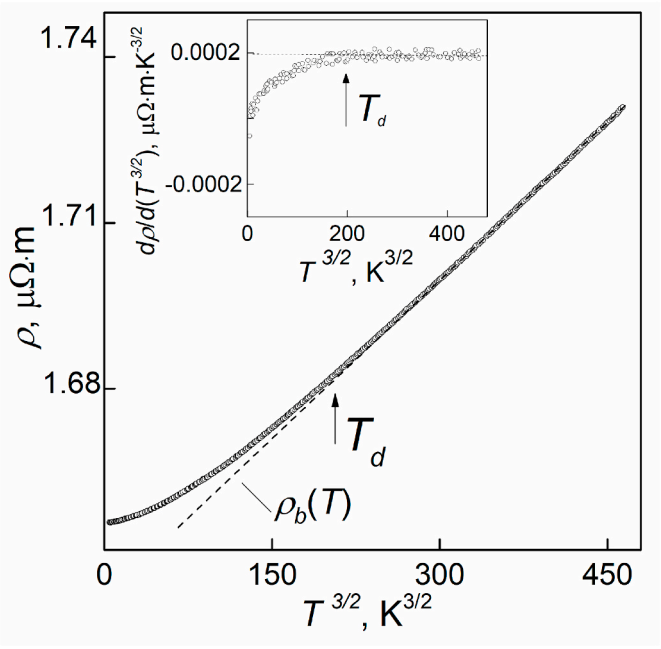

Fig. 3. The $\rho(T^{3/2})$ dependence taken at $j = 280{\cdot}10^4$ A·m^{-2}. Inset: the $d\rho/d(T^{3/2})$ vs. $T^{3/2}$ dependence.

on ρ to the negative one (Fig. 2 (b)). This temperature can be taken as a characteristic temperature that divides the low- and high-temperature ranges in the $\rho(T)$ behavior. Thus, within the high-temperature range, the $\rho(T)$ behavior of the compound being studied is dominantly governed by the acoustic phonon scattering.

Below T_d, the acoustic phonon scattering is gradually changed to another conductivity mechanism. To find the $\Delta\rho(T)$ change due to this mechanism, a background contribution into the electrical resistivity for the low-temperature range should be taken into account. Let us believe that this background contribution is dominantly related to the relevant $\rho(T)$ change, characteristic for the high-temperature range. The experimental $\rho(T^{3/2})$ linear dependences can be extrapolated from the high-to low-temperature range, and, hence, below T_d these extrapolated lines can be taken as the background $\rho(T)$ contribution into the total $\rho(T)$ change. Then, subtracting this background contribution from the experimental $\rho(T)$ curves, the $\Delta\rho(T)$ change due to the conductivity mechanism, which is gradually developing below T_d, can be extracted. One can see that for all the j values, $\Delta\rho$ is steady increasing, starting from T_d down to lowest temperature (Fig. 4). Besides, the j-effect on $\Delta\rho(T)$ is gradually decreasing with increasing j.

As was shown earlier [21,22], semiconducting $\rho(T)$ behavior, observed at small currents in $Bi_{1.9}Gd_{0.1}Te_3$ below T_m (inset to Fig. 2 (b)), can be satisfactory described in framework of variable-range hopping (VRH) conductivity mechanism. Thus, one can conclude that at T_d the conductivity mechanism due to the acoustic phonon scattering, which is major one above T_d, starts to be gradually changed to the VRH conductivity mechanism, and already the VRH conductivity mechanism becomes dominant one below T_m.

To characterize the features in the electrical properties, which is related to changing in the conductivity mechanisms, let us analyze the $\rho(j)$ dependences, measured in accordance with the second measuring mode. To compare these dependences taken at various temperatures, the $\rho(j)$ changes were again used to calculate $DCR = [\rho(j_{max}) - \rho(j_{min})]/\rho(j_{min})$. Fig. 5 shows the $DCR(j)$ dependences, taken for the high-temperature range at $T > T_d$ (upper panel), and for the low-temperature range at $T \leq T_d$ (bottom panel). For the high-temperature range, corresponding to the acoustic phonon scattering, DCR is positive (DCR^+), whereas for the low-temperature range, corresponding to changing in the conductivity mechanism to the VRH mechanism, DCR is negative (DCR^-). At $T = T_d$, the resistivity happens to be practically j-independent. Hence, DCR is equal to zero (the $DCR(j)$ dependence for T_d is positioned on boundary between upper and bottom panels). DCR was found to be strongly T-dependent. Since at sweeping in j, DCR^+ is changed in far strong manner than DCR^-, different DCR scales was used to present DCR^+ and DCR^- at the same Fig. 5.

With decreasing temperature, the T-effect on DCR^+ is gradually weakened at T tending to T_d within the high-temperature range, and the T-effect on DCR^- is remarkably enhanced at T moving away from T_d within the low-temperature range. For following analysis of the DCR^+ and DCR^- behavior, it would be more comfortably to use the electric field strength instead of j (as was mentioned above, j and E are connected to each other via the Ohm law).

Increasing in ρ with gradually enhancing E in some semiconductors can be originated from saturation of drift velocity, v_d, of carriers [2]. For

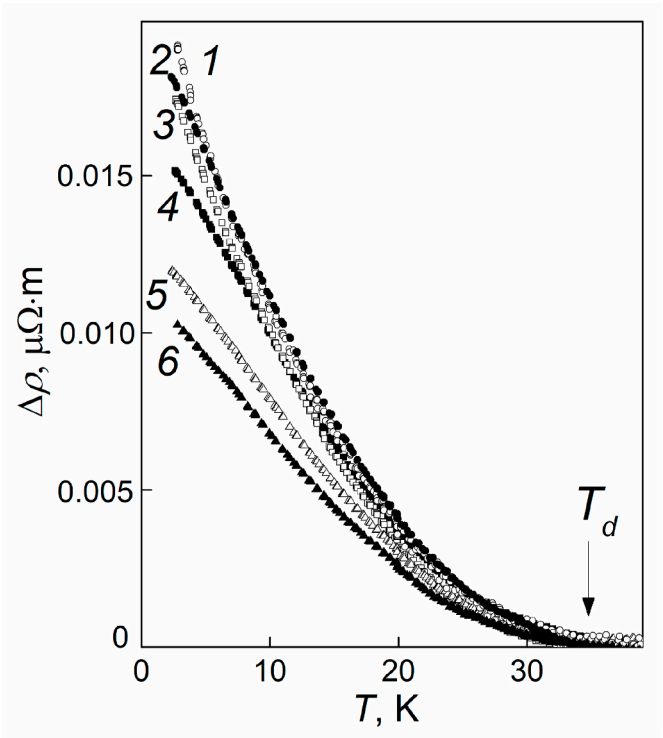

Fig. 4. The $\Delta\rho(T)$ contributions taken at j equal to $9{\cdot}10^4$ (curve *1*), $29{\cdot}10^4$ (*2*), $44{\cdot}10^4$ (*3*), $88{\cdot}10^4$ (*4*) $177{\cdot}10^4$ (*5*) and $280{\cdot}10^4$ A m^{-2} (*6*).

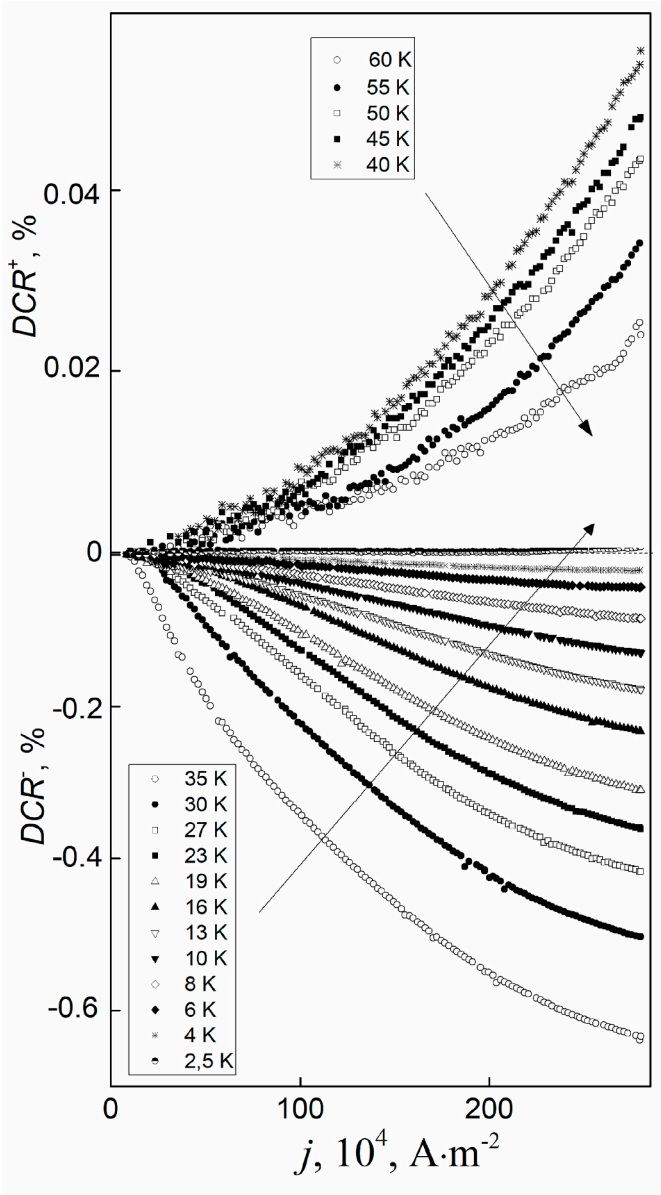

Fig. 5. The $DCR(T)$ dependences taken at various temperatures, corresponding to positive DCR^+ (a) and negative DCR^- (b).

weak electric field, the carrier mobility should be *E*-independent, and then v_d is directly proportional to the electric field in accordance with expression [1].

$$v_d(E) = \mu E \tag{3}$$

The *E*-effect on ρ is observed, when the applied electric field is strong enough and an interaction of carriers with lattice vibrations results in decreasing in the carrier mobility. As result, a non-linear variation of the drift velocity will take place. Generally, with increasing *E*, the drift velocity is also increasing towards a maximum value, v_S, called the saturation velocity. The saturation velocity is important characteristic of the semiconductors, and it is strongly dependent of doping or impurity levels and temperature. Thus, the $\mu(E)$ effect can dominantly contribute into the $DCR^{+}(j)$ dependences (upper panel in Fig. 5). Further, these dependences, as well as results of examination of the Hall effect, were further used to get the $\mu(E)$ dependences.

The $\mu(E)$ dependences, in which μ is reduced by μ_0, taken for temperatures of 60, 55, 50, 45 and 40 K are plotted in Fig. 6 (μ_0 is the carrier mobility, which is corresponding to minimal electric field). By now, a few mathematical expressions were proposed to describe the *E*-effect on μ, but no one can be taken as reference law. To fit the experimental curves presented in Fig. 5, the following empirical expression, earlier proposed in Refs. [2], was applied

$$\mu(E) = \frac{\mu_0}{\left(1 + \left(\frac{E}{E_C}\right)^{n+1}\right)^{1/n}} \tag{4}$$

where E_C and n are the fitting constants.

In accordance with Ref. [2], n can be taken equal to 1 or 2 for a best fitting the experimental data. It was found that expression (4) with $n = 1$ can be really applied to describe the experimental $\mu(E)$ dependences, since the fitting curves (the solid curves in Fig. 6) very well reproduce the experimental data. The $E_C(T)$ dependence, extracted from the fitting procedure, is also shown in inset to Fig. 6. This dependence is rapidly growing with decreasing temperature. The E_C constant is related to the saturation velocity via expression [2].

$$E_C = \frac{v_S}{\mu_o}. \tag{5}$$

The acoustic phonon scattering is weakened with decreasing temperature that results in increasing in the electron mobility (expression 2). As result, v_S and, hence, E_C, will be also increased with decreasing temperature down to 40 K. Below this temperature, additional conductivity mechanism is gradually contributing into the total $\rho(T)$ behavior.

Let us consider main features in the $\rho(E)$ dependences, characteristic for this mechanism. The $\rho(E)$ dependences taken for 23, 13 and 2.5 T are presented in Fig. 7. These dependences are rather complicated. Particularly, an inflection point, E_{cr}, is observed in all the dependences. To find E_{cr}, the $d\rho/dE$ derivative versus *E* dependences were plotted (insets to Fig. 7). The inflection point is corresponding to minimum in these dependences. So, E_{cr} can be considered as a crossover field, dividing two parts in the $\rho(E)$ curves. The $\rho(E)$ dependences were found to be very well fitted by following empirical expression

$$\rho(E) = \rho_i(0) + \rho_{0i} exp\left(-\frac{E}{E_i}\right) \tag{6}$$

where $\rho_i(0)$, ρ_{0i} and E_i are the fitting constants.

It is important to note that the expression (6) can be applied to describe the experimental $\rho(E)$ dependences as below E_{cr} and above E_{cr}. But, ρ_{0i} and E_i are negative for $E < E_{cr}$ (in this case $i = 1$), whereas for $E > E_{cr}$ these constants are positive ($i = 2$). The fitting curves, corresponding to expression (6), are shown as the solid curves in Fig. 7. The $E_{cr}(T)$, $E_1(T)$ and $E_2(T)$ dependences, extracted from the fitting procedure, are shown in Fig. 7. For all the measuring temperatures, the experimental $\rho(E)$ dependences include two contributions with E_1 for $E < E_{cr}$, and with E_2 for $E > E_{cr}$. These contributions are separated by E_{cr}. The crossover field was found to be gradually shifted to lower electric fields with decreasing temperature (curve *1* in Fig. 8). It means that at $T \to 35$ K, the contribution with E_1 is dominant, whereas at $T \to 2.5$ K the contribution with E_2 is gradually becoming major one. Generally, the VRH conductivity, which was earlier involved to describe the semiconductor $\rho(E)$ behavior in $Bi_{1.9}Gd_{0.1}Te_3$ below T_m, can be activated by as the temperature and the electric field [3,21,26]. This activation enhances energy of electron that is hopping from an initial localized state to a final localized state. These localized states are positioned inside an impurity band. Under the electric field activation, range of accessible energies of the final localized states can be remarkably broadened. As result, more states near the initial localized state become available for the electron hops.

Usually, the *E*-activation of the VRH conductivity under weak electric field results in an exponential decay in the electric resistivity with increasing electric field [3,21,26]. The $\rho(E)$ curves taken for $Bi_{1.9}Gd_{0.1}Te_3$ within the low-temperature range can be also fitted by the exponential decay law (expression 6). The E_1 and E_2 parameters characterize ability of the electric field to activate the VRH conductivity. The first parameter is gradually increasing with decreasing temperature (curve *2* in Fig. 8). The second parameter behaves in more complicated manner (curve *3*). With decreasing temperature, E_2 is firstly increasing down to temperature of ~20 K, and then starting to fall. At present, to explain the features in the $E_1(T)$ and $E_2(T)$ behavior is rather difficult task. Further experiments should be carried out.

The contribution with E_1 can be likely attributed to the acoustic phonon scattering, which is dominant conductivity mechanism for the high-temperature range. With decreasing temperature, this mechanism is effectively depressed by the VRH conductivity mechanism (the contribution with E_2), which is gradually developing within the low-temperature range. Nevertheless, the acoustic phonon scattering seems to retain within the low-temperature range. The acoustic phonon

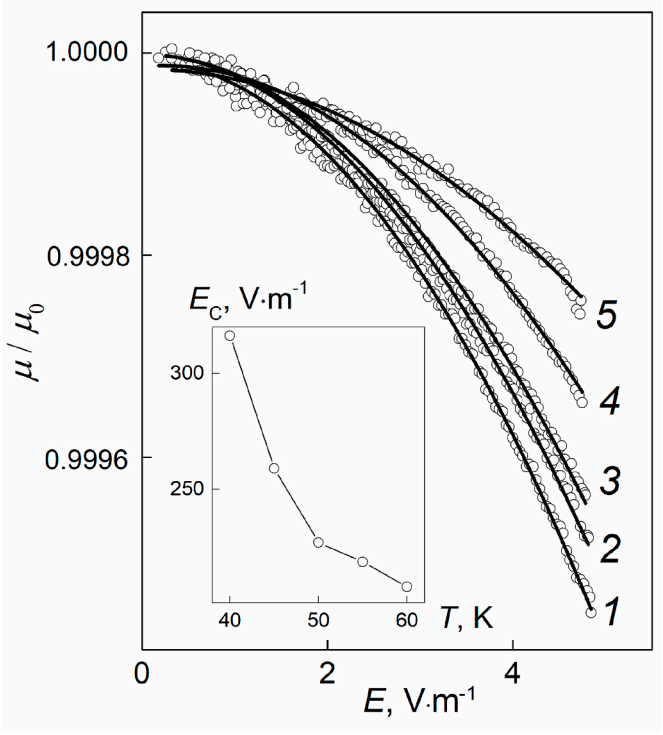

Fig. 6. The $\mu/\mu_0(E)$ dependences taken at temperatures equal to 60 (curve *1*), 55 (*2*), 50 (*3*), 45 (*4*) and 40 K (*5*); solid curves are the fitting curves obtained by expression (4). Inset: the $E_C(T)$ dependence.

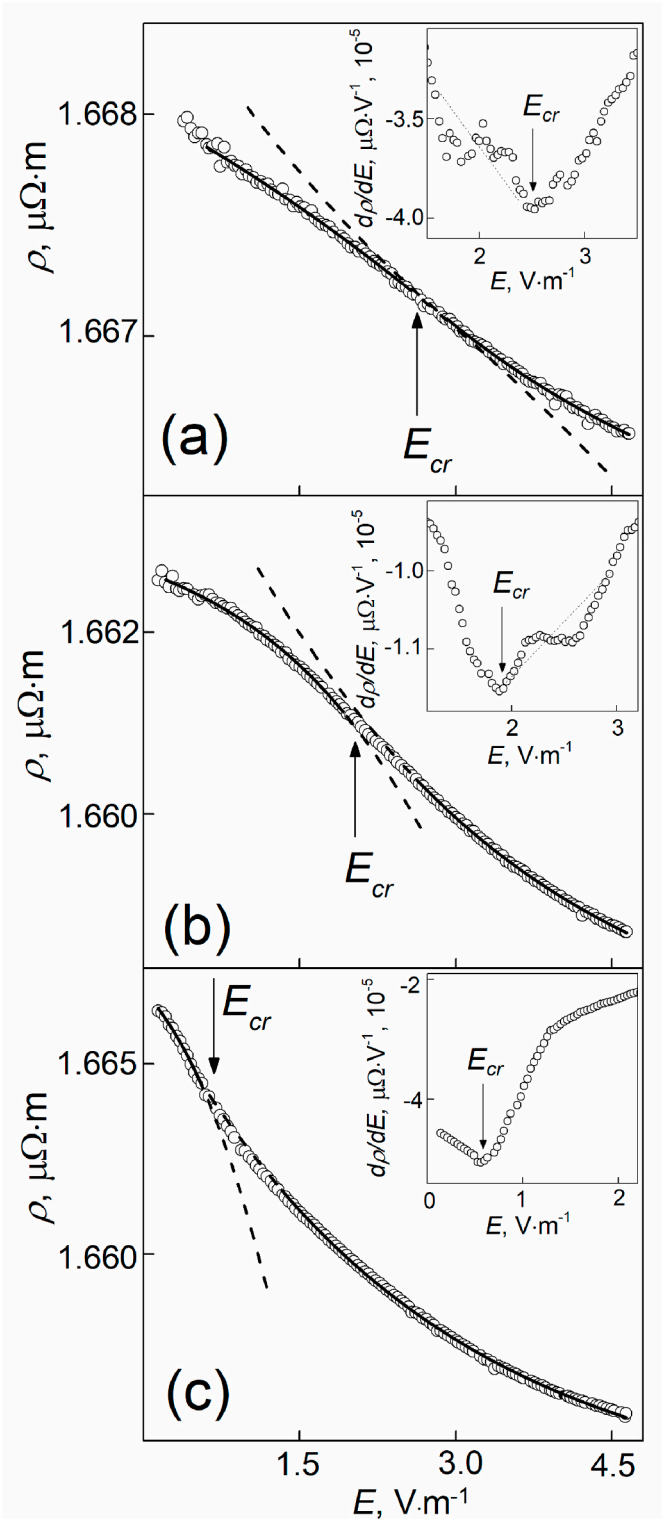

Fig. 7. The $\rho(E)$ dependences taken at temperatures equal to 23 (a), 13 (b) and 2.5 K (c); solid curves are the fitting curves, obtained by expressions (6) for $E < E_{cr}$ and $E > E_{cr}$. Insets: the relevant $d\rho/dE$ vs. E dependences.

scattering results in metal (ρ is decreasing with decreasing temperature) behavior in the electrical resistivity, whereas semiconducting (ρ is increasing with decreasing temperature) behavior is characteristic for the VRH conductivity. At lowest temperatures, the contribution from the acoustic phonon scattering becomes to be neglectable, and the semiconducting behavior in ρ is dominant.

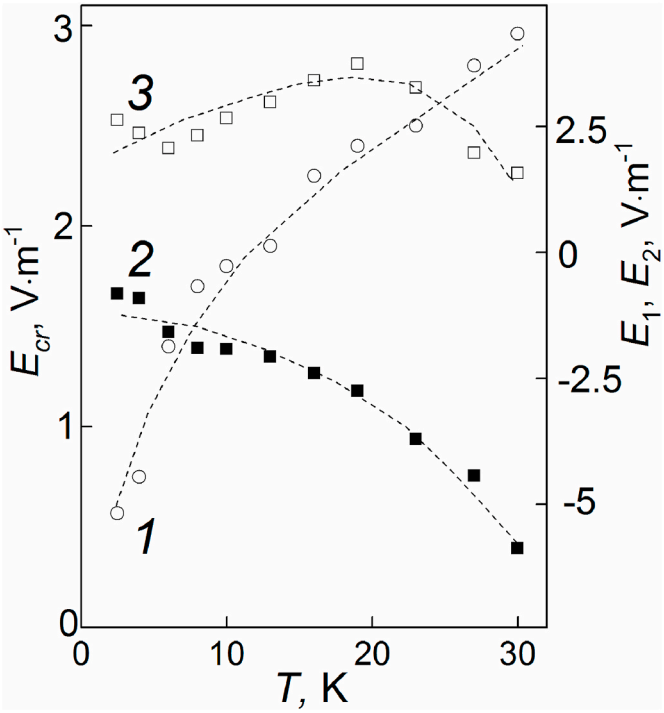

Fig. 8. The temperature dependences of E_{cr} (curve *1*), E_1 (*2*) and E_2 (*3*) for the low-temperature range.

It should be noted that besides the VRH conductivity, other conductivity mechanisms, like an electron-electron scattering [1,27,28] or a scattering by ionized impurities [1,28,29], could be also result in semiconducting behavior in ρ, observed in the sample being studied at low temperatures. There are several reasons to take the VRH conductivity to analyze the features in low-temperature electrical properties of $Bi_{1.9}Gd_{0.1}Te_3$. Firstly, the temperature and magnetic field behavior of the electrical resistivity is in agreement in the VRH conductivity mechanism [21,22]. Secondly, the linear positive magnetoresistance was found in $Bi_{1.9}Gd_{0.1}Te_3$ [23]. On the one hand, the linear magnetoresistance is characteristic of disordered and inhomogeneous semiconductors [30–32]. On the other hand, the VRH conductivity is also characteristic of disordered and inhomogeneous semiconductors [26]. Usually, the $\rho(T)$ changes, related to the VRH conductivity, is expressed in much more manner, as compared to the relevant $\rho(T)$ changes in $Bi_{1.9}Gd_{0.1}Te_3$. However, the VRH conductivity can always take place in disordered and inhomogeneous semiconductors [26]. As a rule, other conductivity mechanisms mask the VRH conductivity. To effectively implement the VRH conductivity, a few parameters, like a width of the impurity band, overlapping this band with conductance (valence) band, position of the Fermi level, the features in the density of states etc., should be suitably combined in semiconductor. So, one can believe that specific combination of these parameters in $Bi_{1.9}Gd_{0.1}Te_3$ can really result in very weak VRH conductivity at low temperatures, and the relevant $\rho(T)$ changes will be minor. Finally, as was mentioned above, rare earth elements like Lu, Ce, Sm, Er, La enhance the thermoelectric figure-of-merit of Bi_2Te_3. This enhancement is assumed to be originated from forming the narrow and non-parabolic impurity band lying near the Fermi level with high and sharp density of states, which is related to rare earth elements. In this case, both scattering factor and density-of-states effective mass of carriers could be remarkably enhanced, that results in increasing in the Seebeck coefficient, and, hence, in the thermoelectric figure-of-merit [33,34]. Besides increase in the Seebeck coefficient, the impurity band can remarkably effect on low temperature electrical conductivity of thermoelectrics. Particularly, the impurity band can result in hopping conductivity onset, when electron

gets ability to tunnel from one to another localized state within the impurity energy band. Thus, the impurity Lu band can be responsible for enhancing in the thermoelectric figure-of-merit in the Lu-doped Bi_2Te_3. The same impurity band can also result in the VRH conductivity at low temperatures.

4. Conclusion

Thus, low temperature resistivity of *n*-type $Bi_{1.9}Lu_{0.1}Te_3$ compound has been found to be dependent on the measuring electric current. Within the high-temperature range, corresponding to metal behavior in the resistivity, the *j*-effect on ρ is positive, i.e. the resistivity is growing with increasing current. The positive effect can be attributed to saturation of the drift velocity of electrons at the acoustic phonon scattering. Within the low-temperature range, the negative *j*-effect on ρ (the resistivity is falling with increasing current) was observed. In this case, the acoustic phonon scattering is gradually depressed by other conductivity mechanism, which results in semiconducting behavior in ρ. The variable-range hopping conductivity is considered as other mechanism. Under the electric field activation, the resistivity for the hopping conductivity mechanism is gradually decreasing with increasing in the electric field strength. Competition between the acoustic phonon scattering and the VRH conductivity results in appearance of minimum in the resistivity at low temperatures.

CRediT authorship contribution statement

Oleg Ivanov: Conceptualization, Writing - review & editing. **Maxim Yaprintsev:** Formal analysis, Writing - original draft, Investigation.

Declaration of competing Interest

The authors declare that they have no known competing financial interests or personal relationships that could have appeared to influence the work reported in this paper.

References

[1] J.S. Blakemore, Solid State Physics, Cambridge University Press, Cambridge, 1985.
[2] M. Azizi, C. Azizi, M. Zaabat, Effect of the electric field on the carrier mobility for GaAs MESFET's with submicrone gate, J. Electron. Dev. 22 (2015) 1880–1887.
[3] G.K. van Ancum, M.A.J. Verhoeven, D.H.A. Blank, H. Rogalla, Electric-field activated variable-range hopping conductivity in $PrBa_2Cu_3O_{7-\delta}$, Phys. Rev. B 52 (1995) 5598–5602.
[4] K. Alfaramawi, Electric field dependence of the electron mobility in bulk wurtzite ZnO, Bull. Mater. Sci. 37 (2014) 1603–1606.
[5] S. Baranovskii, O. Rubel, Charge transport in disordered materials, in: S. Kasap, P. Capper (Eds.), Springer Handbook of Electronic and Photonic Materials, Springer Handbooks. Springer, Cham, 2017.
[6] H.J. Goldsmid, Bismuth telluride and its alloys as materials for thermoelectric generation, Materials 7 (2014) 2577–2592.
[7] H. Scherrer, S. Scherrer, Thermoelectric properties of bismuth antimony telluride solid solutions, Thermoelectrics Handbook: macro to Nano, in: D.M. Rowe (Ed.), CRC Taylor and Francis, Boca Raton, FL, USA, 2012.
[8] K. Behnia, Fundamentals of Thermoelectricity, Oxford University Press, Oxford, 2015.
[9] Y. Pan, T.R. Wei, C.F. Wu, J.F. Li, Electrical and thermal transport properties of spark plasma sintered n-type $Bi_2Te_{3-x}Se_x$ alloys: the combined effect of point defect and Se content, J. Mater. Chem. C. 3 (2015) 10583–10589.
[10] L. Hu, T. Zhu, X. Liu, X. Zhao, Point defect engineering of high-performance bismuth-telluride-based thermoelectric materials, Adv. Funct. Mater. 24 (2014) 5211–5218.
[11] J. Suh, K.M. Yu, D. Fu, X. Liu, F. Yang, J. Fan, D.J. Smith, Y.H. Zhang, J.K. Furdyna, C. Dames, W. Walukiewicz, J. Wu, Simultaneous enhancement of electrical conductivity and thermopower of Bi_2Te_3 by multifunctionality of native defects, Adv. Mater. 27 (2015) 3681–3686.
[12] J. Yang, F. Wu, Z. Zhu, L. Yao, H. Song, X. Hu, Thermoelectrical properties of lutetium-doped Bi_2Te_3 bulk samples prepared from flower-like nanopowders, J. Alloys Compd. 619 (2015) 401–405.
[13] O. Ivanov, M. Yaprintsev, R. Lyubushkin, O. Soklakova, Enhancement of thermoelectric efficiency in Bi_2Te_3 via rare earth element doping, Scripta Mater. 146 (2018) 91–94.
[14] M. Yaprintsev, R. Lyubushkin, O. Soklakova, O. Ivanov, Effects of Lu and Tm doping on thermoelectric properties of Bi_2Te_3, J. Electron. Mater. 47 (2018) 1362–1370.
[15] O. Ivanov, M. Yaprintsev, Mechanisms of thermoelectric efficiency enhancement in Lu-doped Bi_2Te_3, Mater. Res. Express 5 (2018) 1–10, 015905.
[16] M. Yapryntsev, A. Vasiliev, O. Ivanov, Sintering temperature effect on thermoelectric properties and microstructure of the grained $Bi_{1.9}Gd_{0.1}Te_3$ compound, J. Eur. Ceram. Soc. 39 (2019) 1193–1205.
[17] F. Wu, W. Shi, X. Hu, Preparation and thermoelectric properties of flower-like nanoparticles of Ce-Doped Bi_2Te_3, Electron, Mater. Lett. 11 (2015) 127–132.
[18] F. Wu, H. Song, J. Jia, X. Hu, Effects of Ce, Y, and Sm doping on the thermoelectric properties of Bi_2Te_3 alloy, Prog. Nat. Sci. Mater. Int. 23 (2013) 408–412.
[19] F. Wu, H.Z. Song, J.F. Jia, F. Gao, Y.J. Zhang, X. Hu, Thermoelectric properties of Ce-doped n-type $Ce_xBi_{2-x}Te_{2.7}Se_{0.3}$ nanocomposites, Phys. Status Solidi 210 (2013) 1183–1189.
[20] X.H. Ji, X.B. Zhao, Y.H. Zhang, B.H. Lu, H.L. Ni, Synthesis and properties of rare earth containing Bi_2Te_3 based thermoelectric alloys, J. Alloys Compd. 387 (2005) 282–286.
[21] O. Ivanov, M. Yaprintsev, E. Danshina, Electric field effect on variable-range hopping conductivity in $Bi_{1.9}Lu_{0.1}Te_3$, Phys. B Condens. Matter 545 (2018) 222–227.
[22] O. Ivanov, M. Yaprintsev, Variable-range hopping conductivity in Lu-doped Bi_2Te_3, Solid State Sci. 76 (2018) 111–117.
[23] O. Ivanov, M. Yaprintsev, E. Danshina, Transverse magnetoresistance peculiarities of thermoelectric Lu-doped Bi_2Te_3 compound due to strong electrical disorder, J. Rare Earths 37 (2019) 292–298.
[24] A.B. Pippard, Magnetoresistance in Metals, Cambridge, 1989.
[25] S. Kasap, C. Koughia, H. Ruda, R. Johanson, Handbook of Electronic and Photonic Materials, Springer, Berlin, 2006.
[26] B.I. Shklovskii, A.L. Efros, Electronic Properties of Doped Semiconductor, Springer, Berlin, 1984.
[27] I.S. Beloborodov, A.V. Lopatin, V.M. Vinokur, K.B. Efetov, Granular electronic systems, Rev. Mod. Phys. 79 (2) (2007) 469–518, https://doi.org/10.1103/RevModPhys.79.469.
[28] S.S. Li, Scattering mechanisms and carrier mobilities in semiconductors, in: S.S. Li (Ed.), Semiconductor Physical Electronics, Springer, New York, 2006, pp. 211–245.
[29] L. Pan, S. Mitra, L.-D. Zhao, Y. Shen, Y. Wang, C. Felser, D. Berardan, The role of ionized impurity scattering on the thermoelectric performances of rock salt $AgPb_mSnSe_{2+m}$, Adv. Funct. Mater. 26 (2016) 5149–5157.
[30] R. Xu, A. Husmann, T.F. Rosenbaum, M.L. Saboungi, J.E. Enderby, P.B. Littlewood, Large magnetoresistance in non-magnetic silver chalcogenides, Nature 390 (1997) 57–60.
[31] A. Husmann, J.B. Betts, G.S. Boebinger, A. Migliori, T.F. Rosenbaum, M. L. Saboungi, Megagauss sensors, Nature 417 (2002) 421–424.
[32] J. Hu, T.F. Rosenbaum, Quantum and classical routes to linear magnetoresistance, Nature Matl 7 (2008) 697–700.
[33] H.J. Goldsmid, Impurity band effects in thermoelectric materials, J. Electron. Mater. 41 (2012) 2126–2129.
[34] J.P. Heremans, V. Jovovic, E.S. Toberer, A. Saramat, K. Kurosaki, A. Charoenphakdee, S. Yamanaka, G.J. Snyder, Enhancement of thermoelectric efficiency in PbTe by distortion of the electronic density of states, Science 321 (2008) 554–557.